Advanced Functional Materials

ADVANCED FUNCTIONAL MATERIALS
www.afm-journal.de

RESEARCH ARTICLE OPEN ACCESS

Polymer Infiltration Into SURMOF Channels Enables Hydrophobic and Solid-Like Slippery Functional Thin Films

Angana Borbora[1] | Modan Liu[1] | Hartmut Gliemann[1] | Uttam Manna[2] | Christof Wöll[1]

[1]Karlsruhe Institute of Technology (KIT), Institute of Functional Interfaces (IFG), Eggenstein-Leopoldshafen, Germany | [2]Department of Chemistry and Centre for Nanotechnology, Indian Institute of Technology Guwahati, Guwahati, Assam, India

Correspondence: Uttam Manna (umanna@iitg.ac.in) | Christof Wöll (christof.woell@kit.edu)

Received: 17 November 2025 | **Revised:** 18 January 2026 | **Accepted:** 21 January 2026

Keywords: metal–organic frameworks | polymer infiltration | solid-like SLIPS

ABSTRACT

Designing functional thin films with precisely controlled surface chemistry and smoothness is essential for achieving targeted interfacial properties. Here, we introduce a polymer-chain insertion strategy to fabricate pore-threaded films by grafting uniformly long polymer chains into the vertical channels of surface-mounted metal–organic frameworks (SURMOFs). Using the highly oriented pillared-layer $Cu_2(bdc)_2(dabco)$ SURMOF grown by layer-by-layer deposition as a crystalline host, infiltration of polymer chains into its nanochannels allows systematic tuning of interfacial chemistry and water wettability. Insertion of hydrophobic n-alkane chains effectively masks the polar framework surface, enhances water stability, and imparts strong hydrophobicity. Polymer incorporation leads to characteristic modifications in the X-ray diffraction pattern, and infrared spectroscopy reveals chain alignment through shifts in CH-stretching modes. Notably, films infiltrated with long tetracontane ($C_{40}H_{82}$) chains exhibit lubricant-free slippery behavior, enabling water droplets to slide off readily due to the combination of smooth surface morphology and the low surface energy of exposed hydrocarbon segments. This scalable approach provides an internally integrated method for tailoring SURMOF thin-film properties, expanding their applicability in liquid-repellent coatings, anti-fouling surfaces, and separation technologies.

1 | Introduction

In the past two decades, metal–organic frameworks (MOFs) have emerged as promising materials for gas absorption [1, 2], catalysis [3, 4], and molecular separation [5], owing to their high surface area, porosity, and structural tunability. While the functional behavior of MOFs largely arises from the chemistry within their internal pore environments, much less attention has been devoted to their external surfaces. This is mainly because MOF powders consist of nanometer-sized crystallites, making it difficult to prepare continuous thin films suitable for practical use. As a result, reliable characterization and control of external surface properties- such as water wettability and sliding behavior-are challenging, rendering powder-based MOF films poorly suited for many applications. Various methods have been developed to fabricate uniform, oriented, and scalable MOF thin films [6, 7]. One of the most successful approaches to fabricate well-defined, monolithic MOF thin films is the layer-by-layer (LbL) approach, yielding so-called surface-mounted metal–organic frameworks (SURMOFs) [8–10]. The synthesis involves the LbL deposition of metals and linkers on appropriately functionalized solid substrates [9] and such an approach is also suited for integrating MOFs films into electronic [11], optoelectronic [12], and sensor devices [13]. Furthermore, the post-functionalization of SURMOFs enables a broad range of advanced applications, such as, tailoring of wettability [14, 15], catalysis [16, 17], sensing [18, 19], and separation [20, 21]. Conventional MOF-film surface functionalization approaches rely on

post-synthetic modification of the MOF linkers or metal-oxo nodes in the framework, processes that are often synthetically challenging. For instances, Sun et al. developed an approach to functionalize the metal-oxo nodes of NH_2-UiO-66 MOFs with phenylsilane, resulting in a superhydrophobic NH_2-UiO-66 with enhanced stability and potential for applications such as organic/water separation, self-cleaning surfaces, and liquid marble formation [22]. Bogdanova et al. showed that the amino groups exposed on the surface of monolithic NH_2-UiO-66 MOF thin films can serve as reactive sites for post-synthetic functionalization through a coupling reaction, yielding polymer brushes [23]. The brush-like coiled polymer chains enabled decrease in surface free energy, imparting superhydrophobic properties to the functionalized SURMOFs. However, such post-synthetic modification strategies often result in functionalization limited to the external surface of the MOF films, as the reactant molecules may not effectively diffuse into the porous framework to access internal sites. In addition, the inherently low reactivity of many MOF nodes requires harsh or synthetically challenging conditions, which limits the broader applicability.

Inspired by the Nepenthes pitcher plant, which traps prey using a lubricated porous structure, artificial slippery liquid-infused porous surfaces (SLIPS) are created by infusing porous surfaces with a lubricant oil that forms a stable, smooth liquid layer, providing enhanced water repellency, durability, and reduced adhesion compared to superhydrophobic surfaces [24]. Hydrophobic porous surfaces have traditionally been recognized as ideal candidates for creating SLIPS through lubricant infusion. Similarly, superhydrophobic or hydrophobic MOF films–with their inherent high porosity and surface roughness–serve as excellent platforms for forming SLIPS by being impregnated with fluorinated or silicone lubricants. The lubricants are spontaneously entrapped within the structure by capillary forces and smoothens the porous roughness to impart slippery property [25–28]. The challenges with these approaches involve (1) complicated synthetic procedures, e.g., MOF film functionalization, the identification of suitable combinations of hierarchical textures and lubricants, and (2) the susceptibility of the SLIPS-based surfaces to depletion of the lubricant liquid and droplet cloaking by the lubricant. Considerable efforts have been made to overcome the issues by developing unique nanostructures that retain and redistribute lubricant, thereby delaying its depletion [29], as well as by creating solid-like slippery surfaces. Singh et al. introduced UiO-66-OH MOFs thin films with a hierarchy of nanotextures, and thereafter post-functionalization with alkyl silanes to achieve transparent, robust slippery surface [30]. Previously reported slippery surfaces derived from MOFs mostly involve post-hydrophobic modification followed by lubrication (silicone oil, Krytox, PDMS, etc.) (See Table S1). Here, we aimed to introduce a fundamentally different and facile approach to achieve a robust solid-like slippery interface without requiring traditional post-modification and liquid lubrication processes.

Here, we introduced a novel and facile approach for functionalizing MOF thin films through polymer chain insertion. Previous studies on MOF powders demonstrated absorption of flexible chain compounds of nanoscale length into the cavities of crystalline MOF through favorable π-interactions and thereby allowing their structural characterization [31]. Further, MOF powders have demonstrated that pillared-layer MOF crystals can accommodate various linear polymer chains by threading them through the MOF pore-windows into the nanochannels. This insertion process is driven by favorable interactions with the MOF pore walls that offset the solvation energy as well as the entropic cost of uncoiling, which have been extensively used for polymer recognition and separation [32, 33]. Building on these concepts, we developed a highly oriented pillared-layer $Cu_2(bdc)_2$dabco SURMOF with minimum roughness, fabricated using the LbL deposition technique (Figure 1A). This SURMOF can serve as a matrix for insertion of various types of polymer chains. Insertion was done into the channels running along the (001) crystallographic direction, which are oriented perpendicular to the substrate (see Figure 1B). Under spatial confinement within the pore channels, the alkyl chains adopt extended conformations and protrude from the surface. Thus, the approach enables tailoring of surface chemistry and wettability of inherently hydrophilic MOF films by intercalation of various long-chain polymers–hydrophobic (e.g., alkanes) or hydrophilic (e.g., polyethylene glycol, PEG) into MOF nanopores, offering a highly strategic method to modify MOF thin films from the inside out. For instance, the insertion of hydrophobic polymers such as n-alkanes effectively masks the polar nodes of the framework, transforming the inherently hydrophilic and water-unstable $Cu_2(bdc)_2$dabco SURMOF into hydrophobic materials with significantly improved water stability. In particular, tetracontane (C40)-infiltrated SURMOF films exhibit enhanced hydrophobicity and remarkable slippery behavior, allowing water droplets to easily slide off at inclination. Notably, this solid-like slippery property is achieved without the need for external lubrication due to the inherently smooth (root mean square roughness, Rq~13 nm) surface of the SURMOF combined with the low surface energy imparted by the exposed hydrocarbon chains. This polymer insertion strategy offers a simple, scalable, and internally integrated method for functionalizing MOF films and enhancing water stability, paving the way for the development of stable, lubricant-free slippery surfaces with tunable wettability– thereby advancing their practical application in areas such as anti-fouling, liquid manipulation, and separation technologies.

2 | Results and Discussion

2.1 | Synthesis of Pillared-Layer SURMOF

Crystalline $Cu_2(bdc)_2$dabco SURMOFs were synthesized on gold substrates that were pre-functionalized with a self-assembled monolayer of mercaptoundecanol (MUD) using the LbL deposition of copper(II)acetate, benzene-1,4-dicarboxylic acid (bdc) and 1,4-diazabicyclo(2.2.2)octane (dabco), as shown in Figure 1A [34]. XRD analysis revealed that the resulting SURMOF film possesses a well-defined pillared-layer structure (Figure 1C). The diffractograms obtained in out-of-plane geometry indicate that the film exhibits an almost perfect orientation along the (001) crystallographic direction, perpendicular to the substrate surface, as shown in Figure 1C, red. This preferential growth orientation is further confirmed by in-plane XRD measurements, where all observed diffraction peaks correspond to planes that are perpendicular to the (001) direction (Figure 1C, blue). Slight deviations between the experimentally observed and simulated XRD peak positions may result from sample imperfections or strain effects in

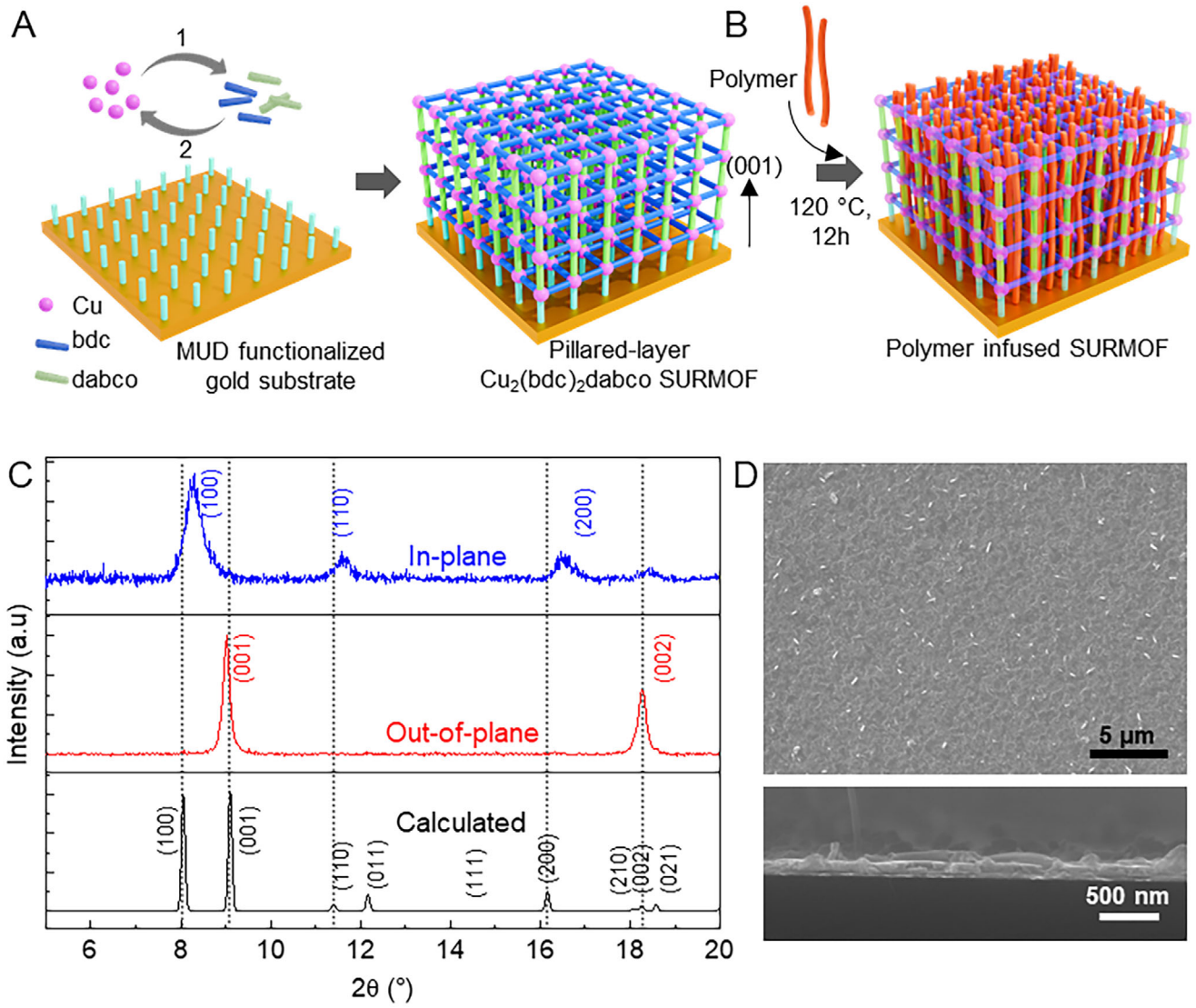

FIGURE 1 | (A) Schematic representation of the synthesis of pillared-layer $Cu_2(bdc)_2dabco$ SURMOF through the LbL deposition of metal and linkers on functionalized gold substrates. (B) Polymer infiltration into the vertical pore channels of the synthesized SURMOF at 120°C for 12 h. (C) Out-of-plane and in-plane diffractograms showing the high degree of orientation of the SURMOFs. For comparison, the calculated powder diffractograms are shown in the lower panel. (D) Scanning electron microscopy images of the synthesized SURMOF film; top view (top) and cross-sectional view (bottom).

the SURMOF. Scanning electron microscopy (SEM) images of the SURMOF reveal the formation of a continuous, monolithic, and uniform thin film with thickness ~100 nm, as shown in Figure 1D. Nonetheless, a small amount of surface defects and nanoscale roughness is present in the surface of the film, as evidenced in magnified SEM and AFM images in Figure S2, which reveal a nano-scale (Rq ~ 13 nm) roughness.

2.2 | Polymer Insertion Into the Nanochannels of SURMOF

In the subsequent series of experiments, we aimed to functionalize the SURMOF film by threading various polymer chains of uniform length–specifically linear alkanes such as eicosane ($C_{20}H_{42}$, referred to as C20), tetracontane ($C_{40}H_{82}$, C40), and polyethylene glycol 1000 (PEG)– into the channels perpendicular to the substrate and along the (001) direction of the SURMOF structure, as shown in Figure 1B [35]. The infusion process was carried out from the polymer melt at 120°C (above the melting temperatures of the polymers), as detailed in the Supporting Information [35]. The synthesized SURMOF demonstrated thermal stability at such temperatures, as indicated by unaltered XRD patterns, as shown in Figure S3. Given the pore dimensions of $Cu_2(bdc)_2dabco$ (approximately 7.5 × 7.5 Å) and considering the molecular cross-sectional thicknesses of the polymers (~ 3.7 Å for linear alkanes and PEG), it is estimated that a maximum of four polymer chains can be accommodated within a single channel [33, 35]. Successful incorporation of the polymers was confirmed using both XRD and infrared reflection-absorption spectroscopy (IRRAS). XRD analysis revealed significant changes in the relative intensities of the diffraction peaks (form factor) upon polymer incorporation. In particular, we analyzed the change in the intensity ratio of the (001) to (002) diffraction peaks following polymer incorporation and observed a significant variation, indicating a modification in the electron density

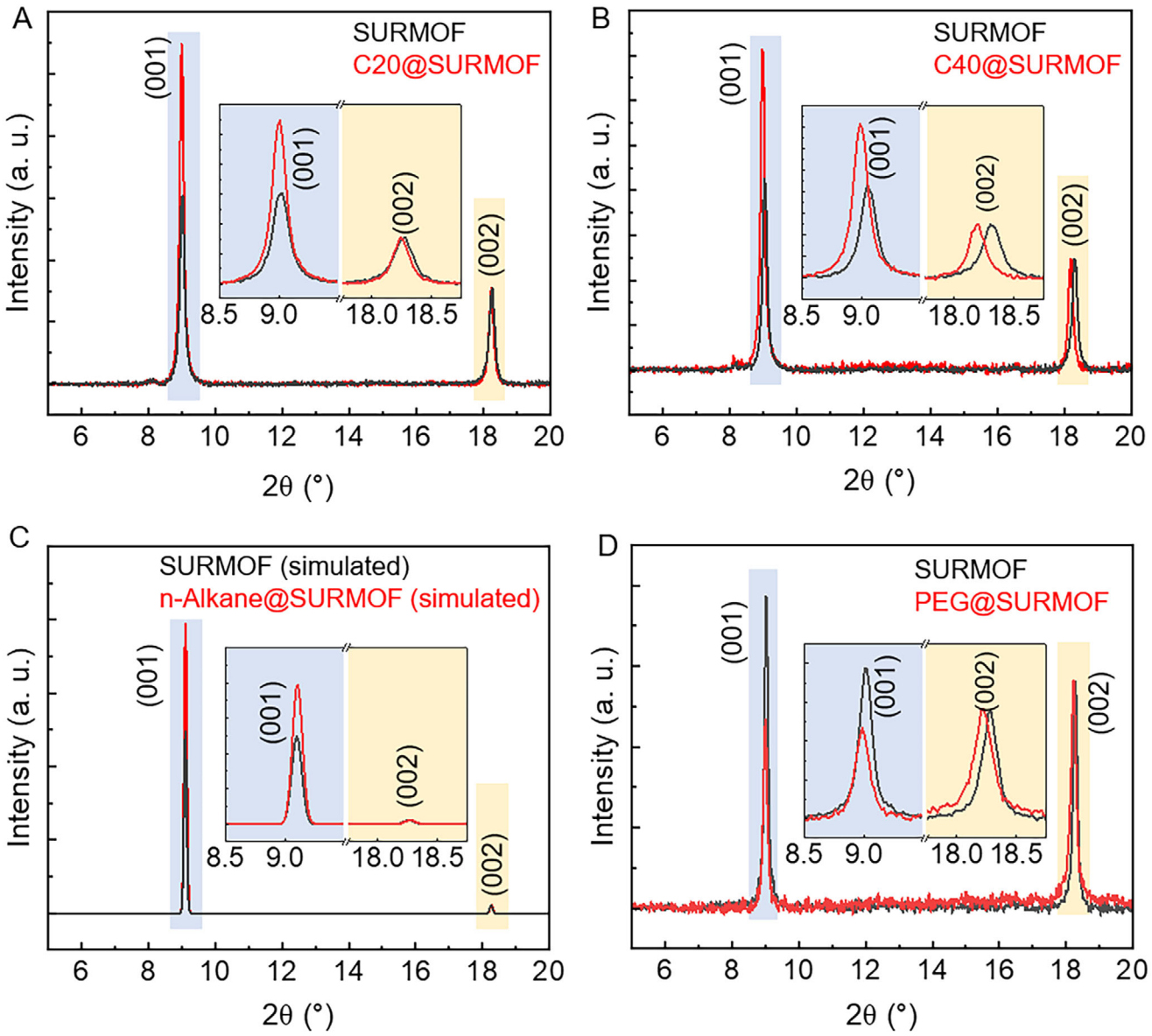

FIGURE 2 | Comparison of out-of-plane XRDs of pillared layer $Cu_2(bdc)_2dabco$ after infusion of (A) C20 and (B) C40, (C) Stimulated out-of-plane XRDs $Cu_2(bdc)_2dabco$ and alkane chain embedded in the pore of $Cu_2(bdc)_2dabco$. (D) Comparison of XRDs of empty and PEG-infused $Cu_2(bdc)_2dabco$.

distribution within the framework [36]. Specifically, the intensity of the (001) peak increased by ~80% upon incorporation of C20 (Figure 2A) and by 68% (Figure 2B) with C40, when normalized to the respective (002) peak intensity. We note that these changes in form factor were not reported in the previous works on polymer insertion in pillared layer MOF powders [33, 35].

To gain deeper insight, we calculated the expected change in form factor for a model where a single alkane chain was embedded into a channel along the (001), as shown in Figure S1. Such a single-chain insertion led to an increase of the (001) peak intensity relative to the (002) peak by 60%, as shown in Figure 2C. The observed experimental changes in form factor are in good agreement with the theoretical predictions and suggest uniform occupation of the polymer chains in the MOF unit cells. In contrast, PEG loading resulted in a decrease of the (001) peak intensity by ~40% with respect to (002), this change in form factor also indicates the uniform distribution of the PEG chains in the MOF framework (Figure 2D). However, the opposite trend in form factor change for PEG compared to C20 or C40 is attributed to differences in their interactions with SURMOF channels, through hydrogen bonding and dipole interactions, causing PEG to occupy the framework in a distinct manner. In addition to the form factor change, minor shifts in peak positions towards lower angles were observed in the out-of-plane XRD patterns following polymer loading, indicating a small expansion of the lattice upon polymer insertion. While the peak shift was negligible for C20, C40 induced a pronounced shift from $2\theta = 9.05°$ and 18.3° to 9.00° and 18.18° (Figure 2B), respectively. These results suggest that the framework undergoes a slight expansion to accommodate the polymer chains, forming favorable hydrophobic interactions. The larger shift observed for C40 is attributed to its fully extended chains being roughly twice as long as C20, leading to greater *c*-axis expansion and a more pronounced shift to lower 2θ. PEG also showed a slight peak shift, from $2\theta = 9.02°$ and 18.28° to 9.00° and 18.22° (Figure 2D).

The shift is observed with PEG, indicating a slight deformation of the MOF lattice likely due to hydrogen bonding interactions between the polymer and functional groups of the MOF ligands, reinforcing the polymer-framework interaction. Slight XRD peak shifts to higher angles are also observed in the in-plane XRD, for example, after C40 infiltration with the (100) peak moving from 8.27° to 8.35°, (110) from 11.65° to 11.79°, (200) from 16.54° to 16.70° and (201) from 18.41° to 18.7°, as shown in Figure S4. This shift strongly suggests that the SURMOF framework shrank slightly along the planar directions of the framework to accommodate the polymer chain. A similar peak shift was previously observed for the corresponding infiltration of MOF powder particles [35].

The incorporation of polymers into the SURMOF was further analyzed using IRRAS technique. After C20 and C40 were absorbed into the SURMOF pores, the polymers displayed distinctive CH asymmetric and symmetric stretching bands, which differed from those of the unabsorbed C20 and C40. Notably, these peaks shifted significantly to higher frequencies, indicating a straightening of the polymer chains within the pillared-layer channels of the SURMOF (Figure 3A,B). This suggests a depletion in the population of gauche conformations and a transition to the anti-conformation. For instance, the SURMOF possesses characteristic IR bands at 1630 and 1393 cm^{-1}, corresponding to the vibrations of the coordinated COO– groups in the crystalline $Cu_2(bdc)_2(dabco)$ structure, with no detectable peaks in the CH stretching region (Figure 3A, gray). The infiltration of C40 was confirmed by the appearance of peaks in the CH-stretching region, alongside the characteristic IR peaks of the SURMOF. Notably, these CH peaks are shifted to higher frequencies compared to the CH peaks observed in unabsorbed C40. The CH_2 stretching vibrations shifted from 2846 ($\nu_s CH_2$) to 2849 cm^{-1} and 2913 ($\nu_{as} CH_2$) to 2918 cm^{-1}, respectively, and the CH_3 stretching frequencies shifted from 2954 ($\nu_{as} CH_3$) to 2964 cm^{-1} upon confinement within the SURMOF channels, as shown in Figure 3A. A similar upward frequency shift of the CH vibrations was observed upon C20 infiltration, as shown in Figure 3B. In the case of PEG–inserted SURMOF, when compared to the spectra of the host SURMOF, new peaks appear around 1250 and 1300 cm^{-1}, indicating the linearly extended conformation of PEG chains within the nanochannels, as shown in Figure S5 [33, 37]. These experimental validations, supported by theoretical calculations, demonstrated that this insertion method is an effective approach to infiltrating polymer chains into the synthesized SURMOF vertical channels, where under spatial confinement the polymer chains adopt extended conformations aligned with the channel axis.

2.2.1 | Surface Wettability Modulation

In the next set of experiments, we explored the possibility of modulating the surface wetting properties of functionalized SURMOF thin films through the polymer infusion approach. Previously, the surface wettability of MOF powders and SURMOFs has been modulated through covalent functionalization of ligand side groups using selected small molecules [14, 15, 25–28]. While effective, this approach is inherently limited to MOFs that possess specific functional groups amenable to further chemical modification. In contrast, our current method offers a more broadly applicable and facile alternative by enabling direct insertion of a variety of polymers into the pore channels and presents a straightforward and versatile strategy for tuning surface wetting properties. The pristine $Cu_2(bdc)_2$dabco SURMOF exhibits an inherent static water contact angle (WCA) of 67° ± 1°, indicative of moderately hydrophilic surface behavior (Figure 4A; Figure S6). Upon infusion with the hydrophobic C20 polymer, the surface becomes more hydrophobic, with the WCA increasing to 84° ± 1°. Incorporation of longer alkyl chains, C30 and C40, further enhances hydrophobicity, with WCA increasing to 105° ± 1° and 112° ± 1°, respectively. This increase in WCA is attributed to the extended hydrocarbon chains protruding from the SURMOF surface, reducing surface energy and repelling water more effectively, as shown in Figure 4A. The surface free energy (SFE) of $Cu_2(bdc)_2(dabco)$ SURMOF, determined using the Owens-Wendt-Rabel-Kaelble (OWRK) [38] method, was 45.6 ± 0.6 mN m^{-1}, which decreased to 34.2 ± 1.2 mN m^{-1} after C_{20} infusion and further declined to 22.7 ± 1.0 mN m^{-1} following C_{40} infusion, as shown in Figure 4A (red curve) and Table S2. This lowering in SFE is attributed to the hydrocarbon-like chemistry on the SURMOF surface, resulting from the protruding alkane chains extending from the SURMOF films. As expected, when hydrophilic PEG was infused into the SURMOF, the surface wetting properties changed to superhydrophilic. In this case, water droplets spread rapidly upon contact (Figure S6), resulting in a remarkably low WCA of 3° ± 1° and the SFE is increased to 64 ± 1.3 mN m^{-1}. This study demonstrates an efficient route for post-synthetic modification of SURMOFs, offering a versatile approach to design surfaces with tailored water wettability and SFE through polymer selection and pore-channel engineering.

Interestingly, insertion of hydrophobic alkanes remarkably enhanced the water stability of SURMOFs by shielding the hydrophilic nodes in the framework and preventing water infiltration. The pristine $Cu_2(bdc)_2$dabco SURMOF exhibits extremely low water stability, disintegrating within 2 h of immersion underwater (neutral pH), as indicated by the disappearance of the XRD peaks, as shown in the Figure 4B. In contrast, SURMOFs incorporating alkyl chain polymers are stable underwater for 12 h, as indicated by the unaltered XRD peak intensities in the Figure 4B and S7A. Although a negligible decrease in XRD peak intensity is observed, likely due to water diffusing through the edges (Figure S7B), the crystallinity of the SURMOFs remains intact even after the immersion period. Moreover, the incorporated polymer chains remain securely entrapped within the pore channels and are not removed even after immersion in ethanol at an elevated temperature (40°C for 6 h), as evidenced by the unchanged XRD form factor (Figure S8). Consequently, the infusion of polymer chains not only increases the water repellency but also the overall stability of the MOF thin films.

2.3 | Solid-Like Slippery Property on Polymer Infused SURMOF

In addition to their hydrophobicity, we also examined the slippery behavior of the alkane-chain–inserted SURMOFs. Conventional SLIPS are bioinspired systems designed to exhibit extremely low adhesion, non-stick, and self-cleaning properties. The slipperiness of SLIPS is typically characterized by the sliding angle (SA),

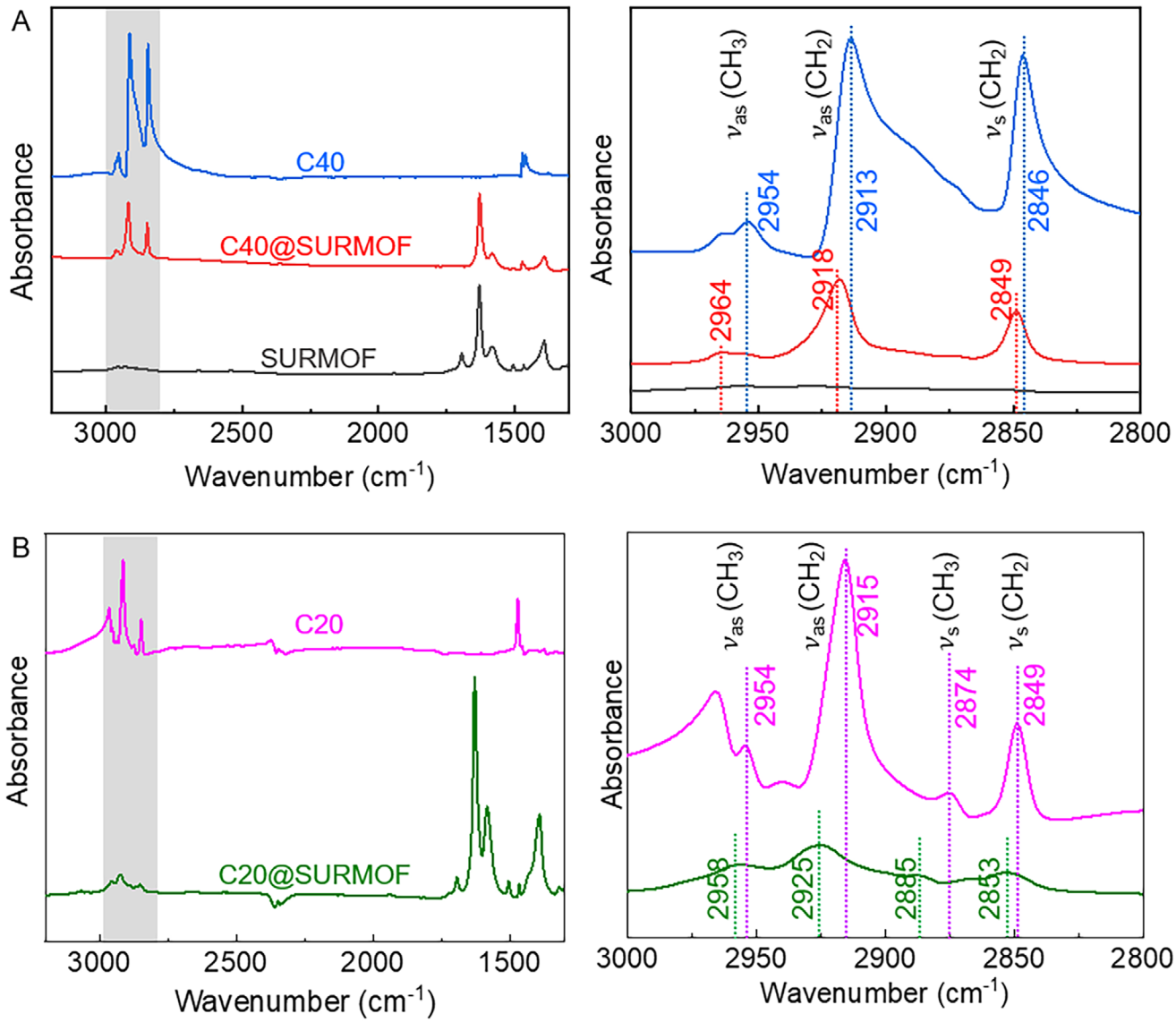

FIGURE 3 | The infrared reflection-absorption spectroscopy (IRRAS) results demonstrate the shift in the CH-region vibration frequency of the alkanes: (A) C40 and (B) C20 after absorption into the SURMOF. The plots on the right side represent a detailed view of the IR bands of the left plots between 3000 and 2800 cm^{-1}.

defined as the tilt angle at which a droplet begins to slide off the surface [24, 26, 39]. Our SURMOF-based system exhibits several advantages over traditional SLIPS systems. Common issues with SLIPS, such as lubricant layer depletion over time and droplet cloaking by the lubricant, could be effectively addressed with the present SURMOF-based approach. The C40-infused SURMOF surface demonstrates excellent slippery behavior without the need for any further lubrication, allowing beaded water droplets to slide off at a tilt angle of 20° (Figures 4C,E; S9), whereas the beaded water droplet pins and spreads on the pristine SURMOF surface due to its inherent hydrophilicity and water instability (Figure 4D). This slippery performance of the C40-infused SURMOF is attributed to the inherently smooth morphology of the SURMOF thin film, with surface roughness (Rq) of ~13 nm, as shown in Figure 4F. Notably, this smoothness is retained even after C40 infusion (Figure 4G). Moreover, the polymers are uniformly absorbed throughout the film surface, as confirmed by SEM images (Figure S10). This uniform and smooth surface minimizes friction during the droplet movement on the surface, a crucial characteristic typically achieved after lubricant infusion in conventional SLIPS. The surface retention force (see Supporting Information for details) is determined to be 660 μNcm^{-2}. Additionally, the extended hydrocarbon chains protruding from the SURMOF surface impart a very low SFE (22.7 ± 1.0 mNm^{-1}, Figure 4A), which further promotes liquid repellency and reduces adhesion. Together, this combination of smooth morphology and hydrocarbon chemistry creates an optimized slippery behavior that mimics SLIPS, without requiring additional lubrication.

However, when we tested a similar surface with twice the amount of C40, the excess deposition (see Supporting Information for details) led to polymer crystallization on the surface, as indicated by the XRD and roughness data in Figure S11A,B. As a result, the surface no longer exhibited slippery behavior (Figure S11C). We suspect that slipperiness is only achieved when the protruding polymer chains are flexible and dangling, rather

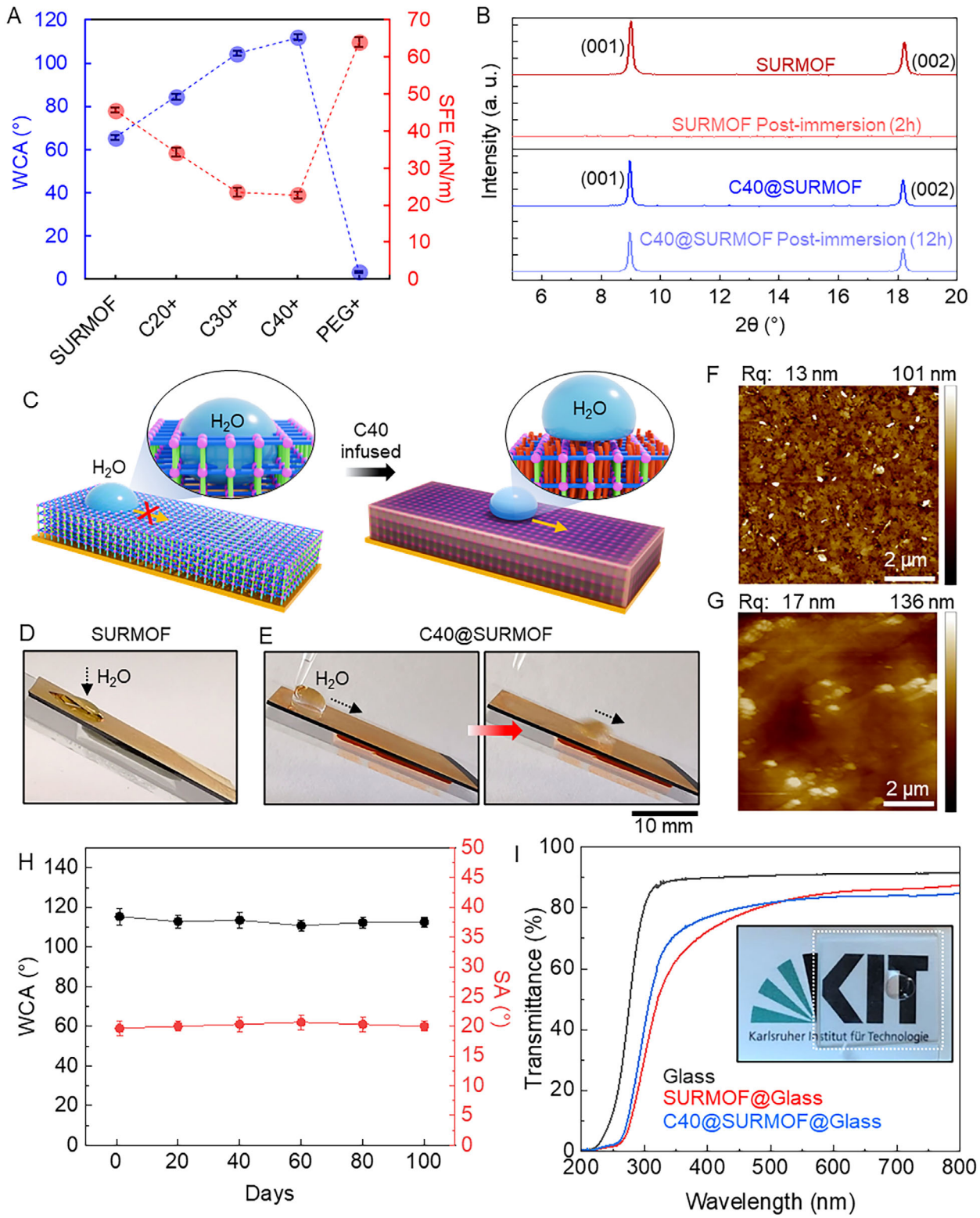

FIGURE 4 | (A) Plot shows the modulation of water contact angle (WCA) and surface free energy (SFE) of $Cu_2(bdc)_2dabco$ SURMOF after incorporation of different polymer chains- C20, C30, C40, and PEG 1000. (B) Out-of-plane XRD patterns for SURMOF and C40@SURMOF, after the specified duration of immersion in water. (C) Schematic representation of the spreading of a beaded water droplet on an inherently hydrophilic $Cu_2(bdc)_2dabco$ SURMOF interface, whereas sliding of the water droplet on the surface after infusion of C40 chain into the vertical channels of the film. (D,E) Digital snapshots showing (D) spreading of a beaded water droplet on $Cu_2(bdc)_2dabco$ SURMOF and (E) sliding of the same on C40@SURMOF. (F,G) AFM images of (F) SURMOF and (G) C40@SURMOF. (H) Graph showing the water contact angle (WCA) and sliding angle (SA) of C40@SURMOF measured at regular intervals over a period of 100 days. (I) Transmittance comparison of C40-infused $Cu_2(bdc)_2dabco$ SURMOF grown on microscope glass, alongside the empty SURMOF film and bare glass substrate. The inset digital image highlights the transparency and slippery nature of the C40@SURMOF@glass placed on a KIT logo at a 20° inclination (See Figure S17).

than crystallized, giving rise to liquid-like slippery. To further understand the origin of the slippery property, we examined the C20-and C30-inserted SURMOF coatings. While both surfaces exhibit comparable surface roughness (Rq = 20.3 and 19.6 nm, respectively, (Figure S12A,B), the C20@SURMOF surface did not exhibit any slippery property, whereas C30@SURMOF showed similar slippery behavior to C40@SURMOF with a sliding angle of 22° for a 20 µL water droplet, as shown in the Figure S12C,D. This could be attributed to the insufficient length of the C20 chain, where all the polymer chains remain beneath the film, leaving no protruding flexible chains on the surface. These experiments revealed that the slippery property depends on the chain length of the inserted polymer and is observed when a sufficient number of flexible chains protrude from the prepared SURMOF. Additionally, we have created a flat C40 film deposited directly on an Au/Si wafer under identical conditions, which also failed to exhibit any slippery property, as shown in Figure S13A. This is likely due to the lack of existence of free chains of polymer. Instead, the hydrocarbon chains crystallized to form solid aggregates (as indicated by XRD pattern, Figure S13B). Eventually, this process introduces heterogeneous surface roughness, as shown in Figure S13C,D. This further highlights the essential role of SURMOF as a host matrix in providing uniform confinement and controlled grafting of polymer chains, enabling solid-like slippery behavior. Moreover, the influence of surface roughness on wetting hysteresis was evaluated by measuring the contact angle hysteresis (CAH) of C30-and C40-infused surfaces with systematically varied roughness, achieved by controlling the deposition amount. The CAH was determined from the advancing and receding contact angles following a previously reported procedure [40]. Rough surfaces exhibit relatively high CAH values (~27°), whereas smoother surfaces show a pronounced reduction in CAH (~11°), as shown in Figure S14. While conventional SLIPS require regular lubricant replenishment due to various depletion mechanisms such as lubricant cloaking, evaporation, and shear-induced loss, our SURMOF-based system maintains consistent hydrophobicity and uninterrupted solid-like slippery performance for over 100 days without any signs of polymer depletion, as shown in Figure 4H. This prolonged slippery performance is a result of the strong interaction between the hydrocarbon chains and the SURMOF thin film and their resistance to leaching. The thermal stability was examined by heating the C40@SURMOF slippery film at 100°C for 12 h, after which it continued to exhibit uninterrupted sliding of water droplets, as shown in Figure S15. Consequently, our system overcomes one of the major limitations of traditional SLIPS, offering a robust and durable slippery performance for practical applications.

Moreover, slippery surfaces possessing high transparency are essential for its relevant applications, such as self-cleaning windows, antifouling surfaces, solar panels, lenses, screens, etc. where both visual clarity and surface functionality are required. To assess the transparency performance of our system, we fabricated $Cu_2(bdc)_2$dabco SURMOF films on microscopic glass substrates, oriented along the (001) direction, via the same LbL deposition approach. Subsequent insertion of C40 led to the expected changes in the form factor, ~72% increase in the intensity of the (001) peak relative to the (002) peak, as shown in Figure S16. Further, we measured the changes in transparency following polymer infusion. The microscopic bare glass showed a transparency of 90%, which decreased slightly to 83% after SURMOF thin film formation, indicating that the oriented crystalline SURMOF film is highly transparent, as shown in Figure 4I. Upon infusion with C40, the transparency remained nearly unchanged at 82% (Figure 4I, blue), while maintaining the slippery property (Figure 4I (inset); Figure S17). Thus, the polymer incorporation into the SURMOF thin films represents a highly effective strategy to introduce functional surface properties while maintaining a high degree of optical transparency—highlighting its potential for multifunctional transparent coatings.

3 | Conclusion

We have successfully synthesized pillared-layer $Cu_2(bdc)_2$dabco SURMOF thin film oriented along the (001) direction via the LbL deposition approach, achieving exceptionally low surface roughness. The resulting SURMOF thin film features vertical channels that enable the insertion of long alkyl polymer chains within the film. Under spatial confinement, the alkyl chains adopt extended conformations aligning to the channel axis, which was thoroughly validated by experimental characterization, supported by the theoretical calculations. The incorporation of hydrophobic n-alkane polymer chains effectively masks hydrophilic nodes of the framework, significantly enhancing the water stability of the films and imparting hydrophobicity. This polymer insertion technique allows to achieve lubricant-free and solid-like slippery property in the SURMOF surface. The synergy of smooth SURMOF morphology with hydrocarbon chemistry creates an optimized solid-like slippery surface that mimics SLIPS behavior without requiring additional lubrication. This scalable and straightforward strategy provides an internally integrated and elegant route to tailor the properties of MOF thin films, thereby advancing their utility and enhancing their potential in liquid-repellent, anti-fouling, self-cleaning coatings, and separation technologies.

Author Contributions

A.B. designed and performed the experiments and wrote the manuscript. M.L. provided molecular dynamics simulations for this work. C.W. supervised the work edited, and reviewed the manuscript. H.G. and U.M. reviewed the manuscript.

Acknowledgements

A.B. and C.W. acknowledge funding by the German Research Foundation (DFG) through the Germany's Excellence Strategy in the context of 3DMM2O. U.M. acknowledges Anusandhan National Research Foundation (CRG/2022/000710; SERB) for financial support. A.B. acknowledges Matthias Barczewski for his support in providing access to the contact angle measurement facility at INT, KIT.

Open access funding enabled and organized by Projekt DEAL.

Conflicts of Interest

The authors declare no conflicts of interest.

Data Availability Statement

The data that support the findings of this study are available in the supplementary material of this article.

References

1. C. A. Trickett, A. Helal, B. A. Al-Maythalony, Z. H. Yamani, K. E. Cordova, and O. M. Yaghi, "The Chemistry of Metal–Organic Frameworks for CO_2 Capture, Regeneration and Conversion," *Nature Reviews Materials* 2 (2017): 17045, https://doi.org/10.1038/natrevmats.2017.45.

2. L. F. Liang, C. P. Liu, F. L. Jiang, et al., "Carbon Dioxide Capture and Conversion by an Acid-Base Resistant Metal-Organic Framework," *Nature Communications* 8 (2017): 1233, https://doi.org/10.1038/s41467-017-01166-3.

3. J. X. Lin, J. Ouyang, T. Y. Liu, et al., "Metal-Organic Framework Boosts Heterogeneous Electron Donor–Acceptor Catalysis," *Nature Communications* 14 (2023): 7757, https://doi.org/10.1038/s41467-023-43577-5.

4. J. Ballesteros-Soberanas, N. Martín, M. Bacic, et al., "A MOF-Supported Pd_1–Au_1 Dimer Catalyses the Semihydrogenation Reaction of Acetylene in Ethylene With a Nearly Barrierless Activation Energy," *Nature Catalysis* 7 (2024): 452–463, https://doi.org/10.1038/s41929-024-01130-7.

5. Z. B. Wang, A. Knebel, S. Grosjean, et al., "Tunable Molecular Separation by Nanoporous Membranes," *Nature Communications* 7 (2016): 13872, https://doi.org/10.1038/ncomms13872.

6. O. Shekhah, J. Liu, R. A. Fischer, and C. Wöll, "MOF Thin Films: Existing and Future Applications," *Chemical Society Reviews* 40 (2011): 1081–1106, https://doi.org/10.1039/c0cs00147c.

7. C. Crivello, S. Sevim, O. Graniel, et al., "Advanced Technologies for the Fabrication of MOF Thin Films," *Materials Horizons* 8 (2021): 168–178, https://doi.org/10.1039/D0MH00898B.

8. L. Heinke and C. Wöll, "Surface-Mounted Metal–Organic Frameworks: Crystalline and Porous Molecular Assemblies for Fundamental Insights and Advanced Applications," *Advanced Materials* 31 (2019): 1806324, https://doi.org/10.1002/adma.201806324.

9. J. L. Zhuang, A. Terfort, and C. Wöll, "Formation of Oriented and Patterned Films of Metal–Organic Frameworks by Liquid Phase Epitaxy: A Review," *Coordination Chemistry Reviews* 307 (2016): 391–424, https://doi.org/10.1016/j.ccr.2015.09.013.

10. C. Scheiger, J. F. Pöhls, M. Mostaghimi, et al., "Dirac-Cone Induced Metallic Conductivity in $Cu_3(HHTP)_2$: High-Quality MOF Thin Films Fabricated via ML-Driven Robotic Synthesis," *Materials Horizons* 12 (2025): 6189–6194.

11. W. J. Li, J. Liu, Z. H. Sun, et al., "Integration of Metal-Organic Frameworks Into an Electrochemical Dielectric Thin Film for Electronic Applications," *Nature Communications* 7 (2016): 11830, https://doi.org/10.1038/ncomms11830.

12. V. Stavila, A. A. Talin, and M. D. Allendorf, "MOF-Based Electronic and Opto-Electronic Devices," *Chemical Society Reviews* 43 (2014): 5994–6010, https://doi.org/10.1039/C4CS00096J.

13. I. Stassen, N. C. Burtch, A. A. Talin, P. Falcaro, M. D. Allendorf, and R. Ameloot, "Correction: An Updated Roadmap for the Integration of Metal–Organic Frameworks With Electronic Devices and Chemical Sensors," *Chemical Society Reviews* 46 (2017): 3853, https://doi.org/10.1039/C7CS90048A.

14. K. Joyaramulu, F. Geyer, A. Schneemann, et al., "Hydrophobic Metal–Organic Frameworks," *Advanced Materials* 31 (2019): 1900820, https://doi.org/10.1002/adma.201900820.

15. J. H. Gu, H. W. Fan, C. X. Li, J. Caro, and H. Meng, "Robust Superhydrophobic/Superoleophilic Wrinkled Microspherical MOF@rGO Composites for Efficient Oil–Water Separation," *Angewandte Chemie International Edition* 58 (2019): 5297–5355, https://doi.org/10.1002/anie.201814487.

16. Z. Jin, D. D. Liu, X. Liu, et al., "Hydrophobic Porphyrin Titanium-Based MOFs for Visible-Light-Driven CO_2 Reduction to Formate," *Inorganic Chemistry* 63 (2024): 1499–1506, https://doi.org/10.1021/acs.inorgchem.3c04241.

17. S. Wang, R. M. Hu, J. Y. Ren, et al., "Surface Hydrophobization of Zeolite Enables Mass Transfer Matching in Gas-Liquid-Solid Three-Phase Hydrogenation Under Ambient Pressure," *Nature Communications* 15 (2024): 2076, https://doi.org/10.1038/s41467-024-46505-3.

18. P. H. F. Fasna and S. Sasi, "A Comprehensive Overview on Advanced Sensing Applications of Functional Metal Organic Frameworks (MOFs)," *Chemistryselect* 6 (2021): 6365–6379, https://doi.org/10.1002/slct.202101533.

19. S. Okur, T. Hashem, E. Bogdanova, et al., "Optimized Detection of Volatile Organic Compounds Utilizing Durable and Selective Arrays of Tailored UiO-66-X SURMOF Sensors," *Acs Sensors* 9 (2024): 622–630, https://doi.org/10.1021/acssensors.3c01575.

20. Y. J. Shan and Q. Liu, "Stimuli-Responsive Metal–Organic Framework (MOF) Separation Membranes: Constructions and Properties," *Industrial & Engineering Chemistry Research* 64 (2025): 3136–3153, https://doi.org/10.1021/acs.iecr.4c04488.

21. X. Li, Y. X. Liu, J. Wang, J. Gascon, J. S. Li, and B. Van der Bruggen, "Metal–Organic Frameworks Based Membranes for Liquid Separation," *Chemical Society Reviews* 46 (2017): 7124–7141, https://doi.org/10.1039/C7CS00575J.

22. D. Sun, P. R. Adiyala, S. J. Yim, and D. P. Kim, "Pore-Surface Engineering by Decorating Metal-Oxo Nodes With Phenylsilane to Give Versatile Super-Hydrophobic Metal–Organic Frameworks (MOFs)," *Angewandte Chemie International Edition* 58 (2019): 7405–7509, https://doi.org/10.1002/anie.201902961.

23. E. Bogdanova, M. D. Liu, P. Hodapp, et al., "Functionalization of Monolithic MOF Thin Films With Hydrocarbon Chains to Achieve Superhydrophobic Surfaces With Tunable Water Adhesion Strength," *Materials Horizons* 12 (2025): 1274–1281, https://doi.org/10.1039/D4MH00899E.

24. T. S. Wong, S. H. Kang, S. K. Y. Tang, et al., "Bioinspired Self-Repairing Slippery Surfaces With Pressure-Stable Omniphobicity," *Nature* 477 (2011): 443–447, https://doi.org/10.1038/nature10447.

25. L. Telmenbayar, A. G. Ramu, D. Yang, and D. Choi, "Development of Mechanically Robust and Anticorrosion Slippery PEO Coating With Metal–Organic Framework (MOF) of Magnesium Alloy," *Chemical Engineering Journal* 458 (2023): 141397.

26. H. R. Li, M. L. Yan, and W. J. Zhao, "Designing a MOF-Based Slippery Lubricant-Infused Porous Surface With Dual Functional Anti-Fouling Strategy," *Journal of Colloid and Interface Science* 607 (2022): 1424–1435, https://doi.org/10.1016/j.jcis.2021.09.052.

27. D. Yang, A. G. Ramu, M. Song, and D. Choi, "Design of a Pillar-Like ZIF-8 Infused Hydrophobic–Slippery Meshes for Highly Efficient Fog Water Harvesting," *Chemical Engineering Journal* 505 (2025): 159001.

28. J. Gao, Y. F. Zhang, W. Wei, et al., "Liquid-Infused Micro-Nanostructured MOF Coatings (LIMNSMCs) With High Anti-Icing Performance," *ACS Applied Materials & Interfaces* 11 (2019): 47545–47552, https://doi.org/10.1021/acsami.9b16181.

29. S. K. Laney, M. Michalska, T. Li, et al., "Delayed Lubricant Depletion of Slippery Liquid Infused Porous Surfaces Using Precision Nanostructures," *Langmuir* 37 (2021): 10071–10078, https://doi.org/10.1021/acs.langmuir.1c01310.

30. V. Singh, X. H. Men, and M. K. Tiwari, "Transparent and Robust Amphiphobic Surfaces Exploiting Nanohierarchical Surface-Grown Metal–Organic Frameworks," *Nano Letters* 21 (2021): 3480–3486, https://doi.org/10.1021/acs.nanolett.1c00157.

31. T. N. Tu and M. Scheer, "A Novel Crystalline Template for the Structural Determination of Flexible Chain Compounds of Nanoscale Length," *Chem* 9 (2023): 227–241, https://doi.org/10.1016/j.chempr.2022.10.016.

32. N. Hosono and T. Uemura, "Metal–Organic Frameworks for Macromolecular Recognition and Separation," *Matter* 3 (2020): 652–663.

33. T. Uemura, N. Yanai, S. Watanabe, et al., "Unveiling Thermal Transitions of Polymers in Subnanometre Pores," *Nature Communications* 1 (2010): 83, https://doi.org/10.1038/ncomms1091.

34. D. H. Chen, H. Gliemann, and C. Wöll, "Layer-by-Layer Assembly of Metal-Organic Framework Thin Films: Fabrication and Advanced Applications," *Chemical Physics Reviews* 4 (2023): 011305, https://doi.org/10.1063/5.0135019.

35. N. Yanai, T. Uemura, and S. Kitagawa, "Behavior of Binary Guests in a Porous Coordination Polymer," *Chemistry of Materials* 24 (2012): 4744–4750, https://doi.org/10.1021/cm3031768.

36. L. Heinke and C. Wöll, "Adsorption and Diffusion in Thin Films of Nanoporous Metal–Organic Frameworks: Ferrocene in SURMOF $Cu_2(ndc)_2(dabco)$," *Physical Chemistry Chemical Physics* 15 (2013): 9295–9299, https://doi.org/10.1039/c3cp50578b.

37. Y. J. Deng, J. B. Dixon, and G. N. White, "Bonding Mechanisms and Conformation of poly(ethylene oxide)-Based Surfactants in Interlayer of Smectite," *Colloid and Polymer Science* 284 (2006): 347–356, https://doi.org/10.1007/s00396-005-1388-0.

38. D. K. Owens and R. C. Wendt, "Estimation of the Surface Free Energy of Polymers," *Journal of Applied Polymer Science* 13 (1969): 1741–1747, https://doi.org/10.1002/app.1969.070130815.

39. X. Yao, Y. H. Hu, A. Grinthal, T. S. Wong, L. Mahadevan, and J. Aizenberg, "Adaptive Fluid-Infused Porous Films With Tunable Transparency and Wettability," *Nature Materials* 12 (2013): 529–534, https://doi.org/10.1038/nmat3598.

40. P. Koochak, M. S. Kiseleva, S. Lepikko, M. Latikka, R. H. A. Ras, and W. S. Y. Wong, "Smoothening Perfluoroalkylated Surfaces: Liquid-Like Despite Molecular Rigidity?," *Advanced Materials Interfaces* 12 (2025): 2400619, https://doi.org/10.1002/admi.202400619.

Supporting Information

Additional supporting information can be found online in the Supporting Information section.

Supporting File: adfm74238-sup-0001-SuppMat.pdf.